Development of Pantograph Electric Field Model for an Electric Train using 3D Finite Element Method

Arak Bunmat[1,*], Pongpisit Saikham[1], Chirayut Nueangrin[1], Tienthong Yuangkaew[1] and Padej Pao-la-or[2]

[1] Department of Electrical Engineering, Rajamangala University of Technology Isan Khonkaen Campus
150 Srichan Road Muang, Khonkaen, Thailand
[2] School of Electrical Engineering, Institute of Engineering, Suranaree University of Technology
111 University Avenue, Mueang Distric, Nakhon Ratchasima, Thailand

arak.bu@rmuti.ac.th[*], pongpisit.sa@rmuti.ac.th, chirayut.nu@rmuti.ac.th, tienthong.yu@rmuti.ac.th and padej@sut.ac.th

Abstract. *This research presents a mathematical model of the electric field of a single-arm pantograph for an electric train. Which is expressed in the form of a second-order partial differential equation. The simulation applied the 3D finite element method developed so that graphical results analyzed the propagation of the electric field around the pantograph system and the contact strip at a voltage of 25 kV and a frequency of 50 Hz. To simulate the single-arm pantograph structure with one upper arm and two upper arms, we can simulate the contact strip being made of graphite material, and the contact strip being made of brass material. It was found that the pantograph in the form of two upper arms had a better electric field dispersion effect than the pantograph in the form of one upper arm. And graphite contact strips have a better electric field dispersion effect than brass contact strips.*

Received by 14 July 2023
Revised by 05 October 2023
Accepted by 24 October 2023

Keywords:

3D finite element method, electric field, pantograph

1. Introduction

With the development of electrified railways at high speeds, pantographs are the main components of the work, transmitting electric power to the propulsion unit. And to complete the electrical cycle, the current will flow through the railway tracks that are grounded. Types of pantographs can be divided into several types; for example, in terms of drive operation, they can be divided into spring-loaded and non-spring-loaded types [1]. In terms of the structure of the lever, it can be divided into both single-arm and double-arm types. In terms of use, it can be divided into both direct current and alternating current [2]. As for the structure of the lever, which is most commonly used today, Z-shaped type pantographs are mostly used as they provide high efficiency in transmitting power and contact with the line. The Z-shape is one of the types of single-arm pantographs. That has been developed to have a more compact size and is designed to respond faster [3]. Single-arm pantographs can be used for almost all types of electric trains, from rail to high-speed trains [4]-[5]. As mentioned above, pantographs are very important for overhead power distribution systems. The research will analyze the structure of a single-arm pantograph for designing high-speed trains that affect the spread of the electric field. It will use two types of single-arm pantograph structures, which use materials in contact strips such as graphite and brass to simulate comparative results [5].

The purpose of this research is to study the effect of the electric field propagation of a single-arm pantograph on 25 kV overhead transmission lines for electric trains [6]. This would be achieved by developing a 3D simulation of the electric field using the finite element method. The researcher has applied the finite element method, which has obvious properties for the design of the workpiece. and structures with complex shapes with precise efficiency, researchers in Thailand and foreign researchers have used the finite element method to calculate the exact solution in each study. Therefore, the researcher uses the finite element method to solve the problem. and calculated the electric field values, analyzing the electric field distribution of single-arm pantographs.

2. Modeling of Electric Field for Pantograph

Internal estimation of 3D elements is the process of selecting the model of the estimation equation within the element. Assuming that the distribution of the solutions on the elements is linear [7]. Therefore, the model of the electric field of the pantograph in 3D can be described as equation (1)

$$\left(\frac{\partial^2 E}{\partial x^2}\right)+\left(\frac{\partial^2 E}{\partial y^2}\right)+\left(\frac{\partial^2 E}{\partial z^2}\right)-\frac{1}{V^2}\left(\frac{\partial^2 E}{\partial t^2}\right)-\mu\sigma\left(\frac{\partial E}{\partial t}\right)=0 \quad (1)$$

From equation (1), considering the 3D problem where V is the propagation velocity of the electric field in terms of relation $V=1/\sqrt{\mu\varepsilon}$, and from the properties of the system Time-Harmonic [7]-[8] can be described as equation (2)

$$\left(\frac{\partial^2 E}{\partial x^2}\right)+\left(\frac{\partial^2 E}{\partial y^2}\right)+\left(\frac{\partial^2 E}{\partial z^2}\right)-\left(j\mu\omega\sigma-\mu\varepsilon\omega^2\right)E=0 \quad (2)$$

3. Resource for Simulation Modeling

3.1 Geometric Modeling Based on SolidWorks

This section outlines the simulation design process for modeling the electric field of a pantograph used in railway applications. We established the study area using a finite element research design, which included generating single-arm pantograph models for electric field calculations [9]. These models are depicted in Fig. 1(a)-(b) and fig. 2(a)-(b).

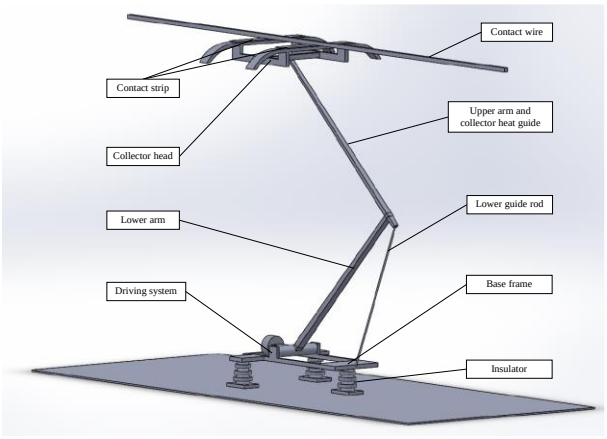

(a) Parts inside the pantograph

(b) Splitting the elements and node

Fig. 1 The single-arm pantograph model, type 1

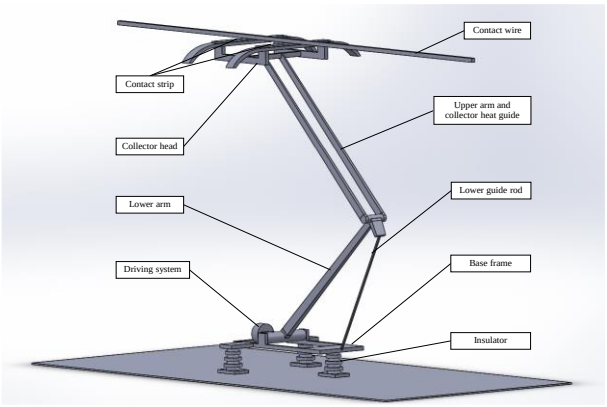

(a) Parts inside the pantograph

(b) Splitting the elements and node

Fig. 2 The single-arm pantograph model, type 2

A structural study of a single-arm pantograph with contact strip, contact wire, collector head, upper arm, lower arm, base frame, driving system, insulation, and air from Fig. 1(a) shows the one-piece upper arm design, and Fig. 2(b) shows the two-piece upper arm design. In the research area, to create the grid to have a resolution or roughness that would change depending on the analytical needs, several grids have been created using the SolidWorks program, which consists of 266,164 elements and 45,693 nodes for pantograph type 1, the result is as shown in Fig. 1(b). and consists of 181,294 elements and 30,989 nodes for pantograph type 2, the result is as shown in Fig. 2(b)

3.2 Development of Finite Element Equations

Assuming the solution distribution characteristics of the elements in a 3D system are linear for solution accuracy, the electromagnetic fields within a tetrahedral element vary linearly at different positions, similar to those of a flat plate [10]. When considering a four-sided, four-point shape, the point-to-point distribution of electric fields results in the following equation: This equation can be used to analyze and predict the behavior of electric fields within such a system [10]-[11].

$$N_n = \frac{1}{6V}\left(a_n + b_n x + c_n y + d_n z\right) \tag{3}$$

The finite element method is widely used to solve a variety of problems and can be further classified based on the method of weighting the residue. Among these methods, the Galerkin method is particularly advantageous because it eliminates the need to choose a position, and the calculation steps are simple and straightforward. Matrices generated using the Galerkin method are often symmetrical, making it ideal for developing computer programs to handle large-scale problems [12]. The Galerkin method has become popular for creating finite element equations. When constructing element equations using the residual weight method, the approximate solution is substituted into the equation, resulting in a non-zero residue value *R*. The residue represents the error between the approximate and exact solutions. The goal is to minimize the residual value *R* to obtain the most accurate approximate solution [13].

For tetrahedron elements, there are 4 unknown points, which means that we need 4 equations to solve for these points. To do this, we typically use a method called Bubnov-Galerkin [14], where we choose the weighting function to be equal to the shape function (W_n=N_n). Using this method, we substitute R as follows: represented by the equation.

$$\int_V N_n \begin{bmatrix} \frac{\partial}{\partial x}\left(\frac{\partial E}{\partial x}\right)+\frac{\partial}{\partial y}\left(\frac{\partial E}{\partial y}\right)+\frac{\partial}{\partial z}\left(\frac{\partial E}{\partial z}\right) \\ -(j\mu\omega\sigma - \mu\varepsilon\omega^2)E \end{bmatrix} dV = 0 \quad (4)$$

Consider the integral term by term. The second derivative term can be evaluated using the method of gradual integration with Gauss's theorem [15]. This method is useful for determining the strength of the electromagnetic field continuously distributed over various objects. If a suitable surface can be defined, the equation can be simplified.

$$\begin{aligned} &\int_V N_n \left[\frac{\partial}{\partial x}\left(\frac{\partial E}{\partial x}\right)+\frac{\partial}{\partial y}\left(\frac{\partial E}{\partial y}\right)+\frac{\partial}{\partial z}\left(\frac{\partial E}{\partial z}\right)\right] dV \\ &-\int_V N_n \left[(j\mu\omega\sigma - \mu\varepsilon\omega^2)E\right] dV = 0 \end{aligned} \quad (5)$$

Consider the left-hand side first term, which is related to the element's scope. Therefore, Neumann boundary conditions for each element must be defined before generating the integrated system load vector equations. After that, Dirichlet conditions are defined to solve the system of linear equations [16]. The finite element equation can then be expressed as:

$$\begin{aligned} &\int_V \left(\left[\frac{\partial N}{\partial x}\right]_{4\times1}\left[\frac{\partial N}{\partial x}\right]_{1\times4}+\left[\frac{\partial N}{\partial y}\right]_{4\times1}\left[\frac{\partial N}{\partial y}\right]_{1\times4}+\left[\frac{\partial N}{\partial z}\right]_{4\times1}\left[\frac{\partial N}{\partial z}\right]_{1\times4}\right) dV [E]_{4\times1} \\ &+\int_V [N]_{4\times1}\left[(j\mu\omega\sigma - \mu\varepsilon\omega^2)[N]_{1\times4}\right] dV [E]_{4\times1} = 0 \end{aligned} \quad (6)$$

To write the finite element equations for each of the four elements, we can use the magnetic permeability matrix (*K*), conductivity matrix (*M*), and current load vector (*F*) [17]. The resulting element-level equation is given as follows:

$$[K+M]_{4\times4}\{E\}_{4\times1} = \{F\}_{4\times1} \quad (7)$$

The magnetic permeability matrix follows:

$$[K]_{4\times4} = \int_V \left(\left[\frac{\partial N}{\partial x}\right]_{4\times1}\left[\frac{\partial N}{\partial x}\right]_{1\times4}+\left[\frac{\partial N}{\partial y}\right]_{4\times1}\left[\frac{\partial N}{\partial y}\right]_{1\times4}+\left[\frac{\partial N}{\partial z}\right]_{4\times1}\left[\frac{\partial N}{\partial z}\right]_{1\times4}\right) dV \quad (8)$$

When substituting the relationship of the equation from the internal approximation function.

$$[K]_{4\times4} = \frac{1}{36V}\begin{bmatrix} b_1b_1+c_1c_1+d_1d_1 & b_1b_2+c_1c_2+d_1d_2 & b_1b_3+c_1c_3+d_1d_3 & b_1b_4+c_1c_4+d_1d_4 \\ & b_2b_2+c_2c_2+d_2d_2 & b_2b_3+c_2c_3+d_2d_3 & b_2b_4+c_2c_4+d_2d_4 \\ & & b_3b_3+c_3c_3+d_3d_3 & b_3b_4+c_3c_4+d_3d_4 \\ Sym & & & b_4b_4+c_4c_4+d_4d_4 \end{bmatrix} \quad (9)$$

The conductivity matrix is calculated from the approximation function and a constant $j\mu\omega\sigma$-$\mu\varepsilon\omega^2$, using an integration formula over the tetrahedral volume [17]-[18].

$$[M]_{4\times4} = \int_V [N]_{4\times1}(j\mu\omega\sigma - \mu\varepsilon\omega^2)[N]_{1\times4}\, dV \quad (10)$$

$$[M]_{4\times4} = (j\mu\omega\sigma - \mu\varepsilon\omega^2)\int_V [N]_n [N]_m\, dV \quad (11)$$

This can be divided into 2 cases: *Nn=Nm* and *Nn≠Nm*; this is also taken into account when examining other tetrahedron junctions. The result is the creation of a conductivity matrix [17]-[18].

$$[M]_{4\times4} = \frac{(j\mu\omega\sigma - \mu\varepsilon\omega^2)}{20}\begin{bmatrix} 2 & 1 & 1 & 1 \\ 1 & 2 & 1 & 1 \\ 1 & 1 & 2 & 1 \\ 1 & 1 & 1 & 2 \end{bmatrix} \quad (12)$$

As external loads are not considered in this analysis, custom-made load current vectors are assumed to be zero. Hence, the effects of the remaining junctions of the tetrahedral geometry are also taken into account [17]-[18].

$$\{F\}_{4\times1} = (0)\int_V [N]_{4\times1}\, dV \quad (13)$$

To obtain the overall equation of the system, the equations of each element are combined. When the study area is divided into sub-elements with n junctions, a system of unified equations comprising all n sub-equations is obtained. This results in the system of linear equations for simulating the electric field intensity effect in this research, where K is the total coefficient of the system, E is the unknown electric field intensity at different node positions, and F is the external force acting at different node positions [18]. The large system equations are as follows:

$$[K]_{n\times n}\{E\}_{n\times1} = \{F\}_{n\times1} \quad (14)$$

3.3 Boundary Conditions and Material Parameter Setting

Incorporate the problem's boundary condition into the system integration equation (constraints). This paper has the initial condition value considered at 25 kV, frequency 50 Hz. Effects of electric fields in both single-arm pantograph structures, with their individual components being all original materials based on the structure [19]-[20]. In the simulation results, the parameters of each material are shown in Table 1 [21]-[22]. To compare the propagation of the electric field in both single-arm pantographs, graphite and brass were used at the contact strip.

Material	Conductivity (σ, S/m)	Relative Permeability (μ_r)	Relative Permittivity (ε_r)
Graphite	$1.0x10^5$	15	0.999999
Brass	$1.59x10^7$	1.0	1.060
Wire (Copper)	$6.0x10^7$	3.5	1
Frame (Steel)	$0.8x10^7$	300	3.5
Insulator	0.1	1.17	8
Air	0	1	1

Table 1 Properties of materials in the simulation [21]-[22]

4. Results and Analysis

We employed a 3D model to simulate the propagation of an electric field, utilizing the structure and contact area of a single-arm pantograph at 25 kV. In this simulation, we considered both graphite and brass contact strip materials. Simulated results for pantograph type 1 are presented in Figures 3(a)-(b) and Fig. 4(a)-(b), while those for pantograph type 2 can be seen in Figures 5(a)-(b) and Fig. 6(a)-(b).

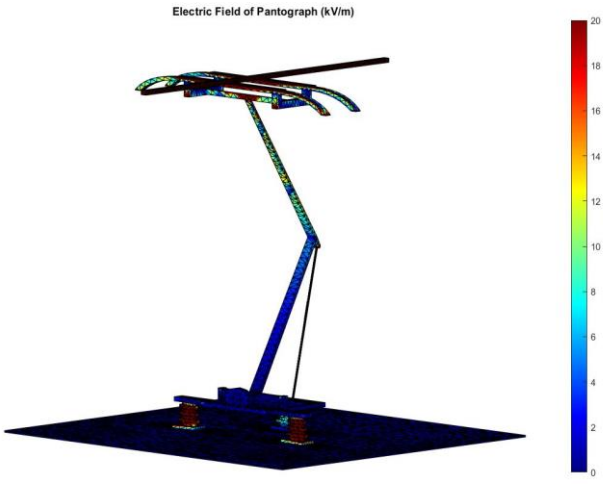

(a) Analysis of electric field distribution in pantograph system

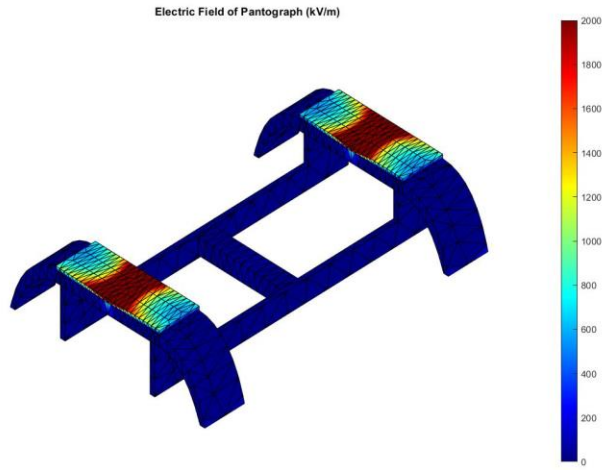

(b) Analysis of electric field distribution in contact strips

Fig. 3 Electric field distribution of the single-arm pantograph type 1, contact strip being made of graphite material

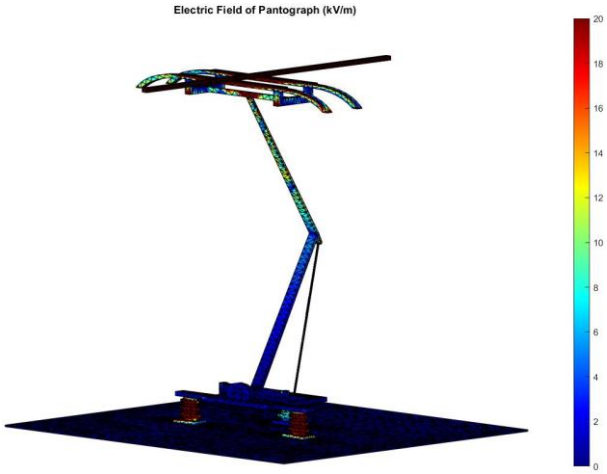

(a) Analysis of electric field distribution in pantograph system

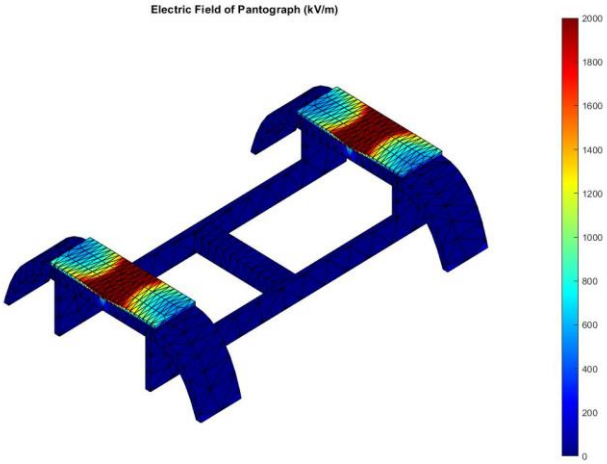

(b) Analysis of electric field distribution in contact strips

Fig. 4 Electric field distribution of the single-arm pantograph type 1, contact strip being made of brass material

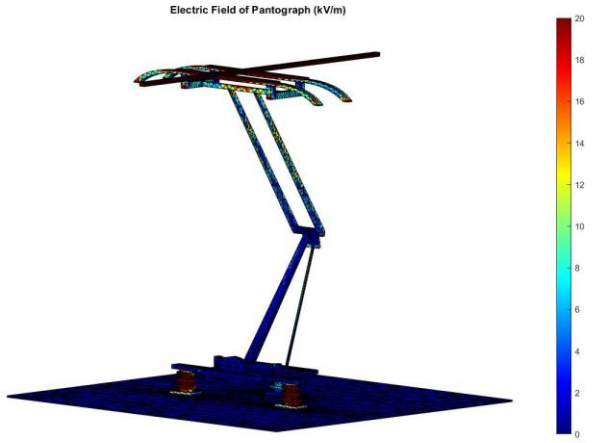

(a) Analysis of electric field distribution in pantograph system

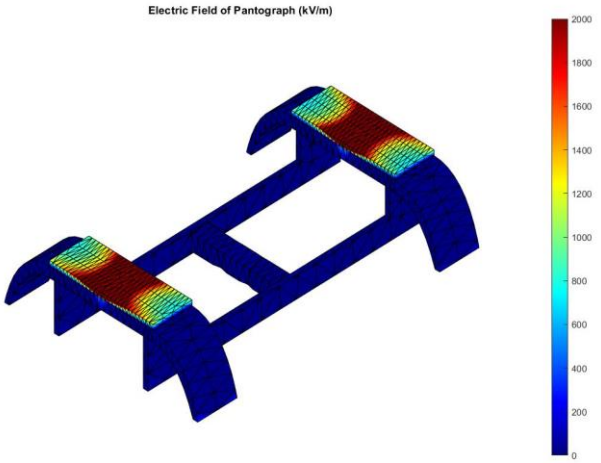

(b) Analysis of electric field distribution in contact strips

Fig. 5 Electric field distribution of the single-arm pantograph type 2, contact strip being made of graphite material

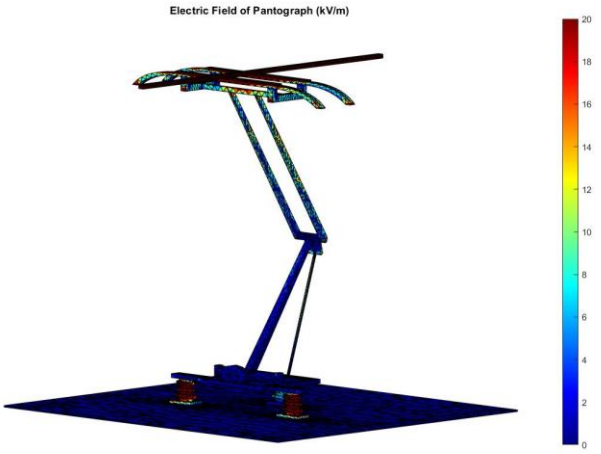

(a) Analysis of electric field distribution in pantograph system

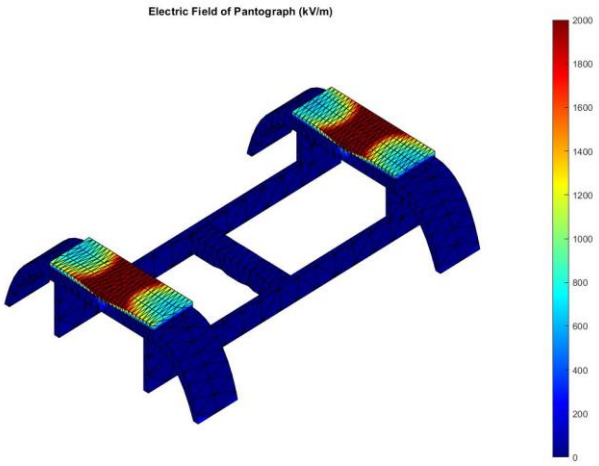

(b) Analysis of electric field distribution in contact strips

Fig. 6 Electric field distribution of the single-arm pantograph type 2, contact strip being made of brass material

The results of the electric field simulation show that the electric field density is highest in the area immediately surrounding the conductor and gradually diminishes as the distance from the conductor increases. Additionally, the electric field spreads around the conductor, resulting in a wider area of impact, as shown in Table 2.

Model	Electric field average (*kV/m*)		Electric field maximum (*kV/m*)	
	Pantograph	Contact strip	Pantograph	Contact strip
Type 1 using graphite	3.1295	1.8769	25	25
Type 1 using brass	3.1232	1.7997		
Type 2 using graphite	3.9097	1.9493		
Type 2 using brass	3.8816	1.7433		

Table 2 Compare the solutions for the electric field distribution

From Table 2, it is found that the electric field in which the contact wire has the maximum electric field value and the area surrounding the contact wire had a lower electric field value with distance from the contact wire. Which in the nearest area was the contact strip, so there was a large distribution of the electric field. Consider the structure of the pantograph in Type 1. The average electric field distribution in the pantograph system when using graphite and brass materials was 3.1295 *kV/m* and 1.8769 *kV/m*, respectively. The average electric field distribution in the contact strip when using graphite and brass materials was 3.1232 *kV/m* and 1.7997 *kV/m*, respectively. And consider the structure of the pantograph in Type 2. The average electric field distribution in the pantograph system when using graphite and brass materials was 3.9097 *kV/m* and 1.9493 *kV/m*, respectively. The average electric field distribution in the contact strip when using graphite and brass materials was 3.8816 *kV/m* and 1.7433 *kV/m*, respectively. Both types of pantographs had maximum electric field of 25 *kV/m*.

5. Conclusions

In this paper, we analyze the suitability of a single-arm pantograph structure for use in electric trains, examining the electric field propagation and contact strip behavior at 25 kV and 50 Hz. We utilized the three-dimensional finite element method (3-D FEM) for our simulations. Our findings indicate that the pantograph with two upper arms performs better in electric field dispersion compared to the single upper arm configuration. Additionally, a comparison between simulations using a graphite contact strip and a brass contact strip reveals that the graphite contact strip exhibits superior electric field dispersion. These simulation results provide valuable insights for further developments aimed at enhancing pantograph efficiency.

Acknowledgements

This work was supported by Faculty of Engineering Contract No. ENG2/66, Rajamangala University of Technology Isan Khonkaen Campus, Thailand

References

[1] M. Mandić, I. Uglešić, and V. Milardić, "Study of Electromagnetic Fields from AC 25 kV/50 Hz Contact Line Systems," *International Review of Electrical Engineering (I.R.E.E.)*, Jan. 2012

[2] G. Aschauer, A. Schirrer, M. Kozek, S. Jakubek, "PHiL pantograph testing via FE-based catenary model with absorbing boundaries," *Control Engineering Practice*, vol. 88, 2019.

[3] T. Li, D. Qin, N. Zhou, J. Zhang, and W. Zhang, "Numerical study on the aerodynamic and acoustic scale effects for high-speed train body and pantograph," *Applied Acoustics*, vol. 196, 2022.

[4] P. Xu, Z. Yang, W. Wei, G. Gao, and G. Wu, "Modeling and Simulation of Arc and Contact Wire Molten Pool Behavior During Pantograph Lowering Process," *AIP Advances*, vol.8 issue11, November 2018.

[5] C. C. Maier, A. Schirrer, M. Kozek, "Real-time capable nonlinear pantograph models using local model networks in state-space configuration," *Mechatronics*, vol.50, 2018.

[6] A. Schirrer, G. Aschauer, E. Talic, M. Kozek, S. Jakubek, "Catenary emulation for hardware-in-the-loop pantograph testing with a model predictive energy-conserving control algorithm," *Mechatronics*, vol.41, 2017.

[7] M.E. El-Hawary, "Electrical Energy Systems," *CRC Press*, USA, 2000.

[8] A. Bunmat, P. Saikham, P. Saeong and W. Tabtaow, "3D Finite Element Analysis of Electric Field for Microwave Oven," *2022 International Electrical Engineering Congress (iEECON)*, Khon Kaen, Thailand, 2022, pp. 1-4.

[9] J. Wu, "Pantograph and Contact Line System," *Academic Press*, China, 2018

[10] S. Tupsie, A. Isaramongkolrak, and P. Pao-la-or, "Analysis of Electromagnetic Field Effects Using FEM for Transmission Lines Transposition," *The World Academy of Science Engineering and Technology*, Tokyo, Japan, vol. 3, no. 5, 2009, pp. 870-874.

[11] A. Bunmat and P. Pao-la-or, "Analysis of magnetic field effects operators working a power transmission line using 3-D finite element method," *2015 18th International Conference on Electrical Machines and Systems (ICEMS)*, Pattaya, Thailand, 2015, pp. 1187-1191.

[12] Jr.W.H. Hayt and J.A. Buck, "Engineering Electromagnetics (7th edition)," *McGraw-Hill*, Singapore, 2006.

[13] M. V. K. Chari and S. J. Salon, "Numerical methods in electromagnetism, " *Academic Press*, USA, 2000.

[14] A. Bunmat, T. Thothumpol. N. Yotphet, and P. Saengsuwan, "Finite Element Analysis of Electric Field Distribution for 115-kV Underground Power Transmission Systems," *International Review on Modelling and Simulations (IREMOS)*, vol. 14, no. 6, 2021, pp. 431-438.

[15] P. Saikham, P. Pao-La-Or, T. Yuangkaew, and A. Bunmat, "Electromagnetic Field Simulation of Pantograph for Electric Train Using 3D Finite Element Method," *2023 International Electrical Engineering Congress (iEECON)*, Krabi, Thailand, 2023, pp. 68-71.

[16] M. Ibrahim and A. Abd-Elhady, "Calculation of Electric Field and Partial Discharge Activity Reduction for Covered Conductor/High Voltage Insulator Systems," *Electric Power Systems Research*, vol. 144, 2017, pp. 72-80

[17] Y. Fan, H. Li, and S. Yang, "Simulation Study on Electric Field Intensity above Train Roof," *AIP Conference Proceedings*, vol. 1955, 2018

[18] P. Pao-la-or, and A. Bunmat, "Shielding of Magnetic Field Effects on Operators Working a Power Transmission Lines Using 3-D FEM," *International Journal of Mechanical Engineering and Robotics Research*, vol. 8, no. 5, Sep. 2019

[19] International Commission of Non-Ionizing Radiation Protection (ICNIRP), "Guidelines for Limiting Exposure to Time-Varying Electric, Magnetic and Electromagnetic Fields (up to 300 GHz), " *Health Phys*, vol. 74, no. 4, 1998, pp. 494-522.

[20] T. Zhao, W. Teng, H. Hao, P. Sun, and Y. Liu, "Simulation Research on Electromagnetic Shielding Characteristics of Carbon Fiber Car Body for Railway Vehicles, " *8th International Congress of Information and Communication Technology (ICICT)*, vol. 154, 2019, pp. 537–542.

[21] A. M. Helmenstine, Ph.D. "Table of Electrical Resistivity and Conductivity, " 2019.

[22] A. Uygun and J. I. Velasco "Electrical Conductivity Modeling of Polypropylene Composites Filled with Carbon Black and Acetylene Black," *International Scholarly Research Network ISRN Polymer Science*, 2012.

Biographies

Arak Bunmat is an assistant professor of the Department of Electrical Engineering, Faculty of Engineering Rajamangala University of Technology Isan Khonkaen Campus, Khonkaen, Thailand. He received B.Eng. (2009), M. Eng. (2013), and D. Eng (2018) in Electrical Engineering from Suranaree University of Technology, Thailand. His fields of research interest include a broad range of power systems, electrical drives, FEM simulation, and artificial intelligence techniques.

Pongpisit Saikham is master's degree student of the Department of Electrical Engineering, Faculty of Engineering Rajamangala University of Technology Isan Khonkaen Campus, Khonkaen, Thailand. His fields of research interest include a broad range of power systems, electrical drives, and FEM simulations.

Chirayut Nueangrin is a PhD student of the Department of Electrical Engineering, Faculty of Engineering Rajamangala University of Technology Isan Khonkaen Campus, Khonkaen, Thailand. His fields of research interest include a broad range of power systems, electrical drives, and FEM simulations.

Tienthong Yuangkaew is a lecturer at Department of Electrical Engineering, Faculty of Engineering, Rajamangala University of Technology Isan Khonkaen campus, Khonkaen, Thailand. He received B.Eng. (2012), and D.Eng. (2020) in Electrical Engineering from Khonkaen University, Thailand. His field of research interest includes a broad range of power system, electrical drives, semiconductor device, nanofabrication, and photoelectrochemical analysis.

Padej Pao-la-or is an associate professor of the School of Electrical Engineering, Institute of Engineering, Suranaree University of Technology, Nakhon Ratchasima, THAILAND. He received B.Eng. (1998), M.Eng. (2002) and D.Eng. (2006) in Electrical Engineering from Suranaree University of Technology, Thailand. His fields of research interest include a broad range of power systems, electrical drives, FEM simulation and artificial intelligent techniques. He has joined the school since December 2005 and is currently a member in Power System Research, Suranaree University of Technology.